Inorganic Chemistry
Article

Inorg. Chem. **2010**, *49*, 9257–9264 **9257**
DOI: 10.1021/ic1007445

Multifunctional Homochiral Lanthanide Camphorates with Mixed Achiral Terephthalate Ligands

Ming-Ling Sun,[†,‡] Jian Zhang,[†] Qi-Pu Lin,[†,‡] Pei-Xiu Yin,[†] and Yuan-Gen Yao*[,†]

[†]*State Key Laboratory of Structural Chemistry, Fujian Institute of Research on the Structure of Matter, Chinese Academy of Sciences, Fuzhou, Fujian 350002, China, and* [‡]*Graduate University of Chinese Academy of Sciences, Beijing 100049, China*

Received April 18, 2010

Seven homochiral lanthanide camphorates with mixed achiral terephthalate ligands, namely, $\{Ln_2(cam)_2(bdc)(H_2O)_2\}\cdot DMF$ [Ln = Sm (**1**), Eu (**2**), Gd (**3**), Tb (**4**), Dy (**5**), Ho (**6**), Er (**7**); D-H_2cam = D-(+)-camphoric acid; H_2bdc = 1,4-benzenedicarboxylic acid; DMF = *N*,*N*′-dimethylformamide], have been solvothermally synthesized. Single-crystal X-ray diffraction analyses reveal that compounds **1**−**7** are isostructural and crystallize in orthorhombic, chiral space group $P2_12_12_1$. These structures feature three-dimensional open frameworks based on rodlike $[Ln_2(OCO)_6(H_2O)_2]_n$ secondary building units, with the guest DMF molecules occupying the void space of the host $\{Ln_2(cam)_3(bdc)(H_2O)_2\}$ framework. The photophysical and magnetic properties of some of these complexes have been investigated. Notably, the terbium compound **4** is highly emissive with a quantum yield of 63.68%. Additionally, thermogravimetric analyses, variable-temperature IR spectrscopy, and powder X-ray diffraction of **2** as a representative were performed to determine its thermal stability, which indicates that the framework still remains intact until 300 °C.

Introduction

Recent successes on the synthesis of homochiral metal−organic framework (MOF) materials have opened up new routes toward applications of enantioselective catalysis, separation, and so forth.[1] One of the most important structural factors for the design of homochiral functional framework materials is the incorporation of enantiopure organic ligands that act as cross-linking or pendent building units. At present, Bu et al. have successfully reported a variety of homochiral MOFs based on enantiopure D-(+)-camphoric acid (D-H_2cam) with many transition metals.[2] Extended metal coordination polymers with open architecture synthesized in the presence of structure-directing agents[3] showed more possibilities in the synthesis of new materials, and no homochiral lanthanide camphorates are known to date. Realizing these points, we have initially explored the construction of chiral lanthanide-containing edifices based on the D-H_2cam ligand as connectors under *N*,*N*′-dimethylformamide (DMF) solvothermal conditions.

As functional metal centers, the technological importance of lanthanide metals[4] has received more and more attention because of their extraordinary coordination properties and

*To whom correspondence should be addressed. E-mail: yyg@fjirsm.ac.cn.

(1) (a) Seo, J. S.; Whang, D.; Lee, H.; Jun, S. I.; Oh, J.; Jeon, Y. J.; Kim, K. *Nature* **2000**, *404*, 982. (b) Kesanli, B.; Lin, W. B. *Coord. Chem. Rev.* **2003**, *246*, 305. (c) Bradshaw, D.; Prior, T. J.; Cussen, E. J.; Claridge, J. B.; Rosseinsky, M. J. *J. Am. Chem. Soc.* **2004**, *126*, 6106. (d) Lin, Z. J.; Slawin, A. M. Z.; Morris, R. E. *J. Am. Chem. Soc.* **2007**, *129*, 4880. (e) Tanaka, K.; Oda, S.; Shiro, M. *Chem. Commun.* **2008**, 820. (f) Ma, L. Q.; Abney, C.; Lin, W. B. *Chem. Soc. Rev.* **2009**, *38*, 1248. (g) Livage, C.; Guillou, N.; Rabu, P.; Pattison, P.; Marrot, J.; Ferey, G. *Chem. Commun.* **2009**, 4551. (h) Clegg, J. K.; Iremonger, S. S.; Hayter, M. J.; Southon, P. D.; Macquart, R. B.; Duriska, M. B.; Jensen, P.; Turner, P.; Jolliffe, K. A.; Kepert, C. J.; Meehan, G. V.; Lindoy, L. F. *Angew. Chem., Int. Ed.* **2010**, *49*, 1075.

(2) (a) Zhang, J.; Yao, Y. G.; Bu, X. H. *Chem. Mater.* **2007**, *19*, 5083. (b) Zhang, J.; Chen, S. M.; Nieto, R. A.; Wu, T.; Feng, P. Y.; Bu, X. H. *Angew. Chem., Int. Ed.* **2010**, *49*, 1267. (c) Zhang, J.; Wu, T.; Feng, P. Y.; Bu, X. H. *Chem. Mater.* **2008**, *20*, 5457. (d) Zhang, J.; Chen, S. M.; Zingiryan, A.; Bu, X. H. *J. Am. Chem. Soc.* **2008**, *130*, 17246. (e) Zhang, J.; Chen, S. M.; Wu, T.; Feng, P. Y.; Bu, X. H. *J. Am. Chem. Soc.* **2008**, *130*, 12882. (f) Zhang, J.; Chen, S. M.; Bu, X. H. *Angew. Chem., Int. Ed.* **2008**, *47*, 5434. (g) Zhang, J.; Bu, X. H. *Chem. Commun.* **2008**, 444. (h) Chen, S. M.; Zhang, J.; Bu, X. H. *Inorg. Chem.* **2008**, *47*, 5567. (i) Zhang, J.; Bu, X. H. *Chem. Commun.* **2009**, 206. (j) Dybtsev, D. N.; Yutkin, M. P.; Peresypkina, E. V.; Virovets, A. V.; Serre, C.; Ferey, G.; Fedin, V. P. *Inorg. Chem.* **2007**, *46*, 6843. (k) Zeng, M. H.; Wang, B.; Wang, X. Y.; Zhang, W. X.; Chen, X. M.; Gao, S. *Inorg. Chem.* **2006**, *45*, 7069. (l) Liang, X. Q.; Li, D. P.; Zhou, X. H.; Sui, Y.; Li, Y. Z.; Zuo, J. L.; You, X. Z. *Cryst. Growth Des.* **2009**, *9*, 4872.

(3) (a) Rao, C. N. R.; Behera, J. N.; Dan, M. *Chem. Soc. Rev.* **2006**, *35*, 375. (b) Mandal, S.; Natarajan, S. *Inorg. Chem.* **2008**, *47*, 5304. (c) Dan, M.; Sivashankar, K.; Cheetham, A. K.; Rao, C. N. R. *J. Solid State Chem.* **2003**, *174*, 60. (d) Behera, J. N.; Rao, C. N. R. *Chem. Asian. J.* **2006**, *1*, 742. (e) Cui, Y.; Ngo, H. L.; Lin, W. B. *Inorg. Chem.* **2002**, *41*, 5940. (f) Boudalis, A. K.; Raptopoulou, C. P.; Abarca, B.; Ballesteros, R.; Chadlaoui, M.; Tachagues, J. P.; Terzis, A. *Angew. Chem., Int. Ed.* **2006**, *45*, 432. (g) Lee, J. Y.; Olson, D. H.; Pan, L.; Emge, T. J.; Li, J. *Adv. Funct. Mater.* **2007**, *17*, 1255. (h) Clausen, H. F.; Poulsen, R. D.; Bond, A. D.; Chevallier, M. A. S.; Iversen, B. B. *J. Solid State Chem.* **2005**, *178*, 3342. (i) Gerardin, C.; Loiseau, T.; Ferey, G.; Taulelle, F.; Navrotsky, A. *Chem. Mater.* **2002**, *14*, 3181.

(4) (a) Bunzli, J. C. G. *Acc. Chem. Res.* **2006**, *39*, 53. (b) Reineke, T. M.; Eddaoudi, M.; O'Keeffe, M.; Yaghi, O. M. *Angew. Chem., Int. Ed.* **1999**, *38*, 2590. (c) Mao, J. G. *Coord. Chem. Rev.* **2007**, *251*, 1493.

Published on Web 09/16/2010

peculiar luminescent and magnetic properties, as well as catalysts and additives in metallurgy. In particular, the luminescent[5] and magnetic properties[6] of achiral lanthanide coordination complexes have been investigated widely during the past decade.[7] However, homochiral lanthanide coordination complexes with interesting magnetic or luminescent properties are rarely reported.[8] It is possible to discover new multifunctional materials by combining homochirality and magnetism or luminescence.

Because there is no large π-conjugated system in homochiral lanthanide camphorates, we attempt to extend this series of linkers to some inherently rigid aromatic spacers, which should effectively enhance the luminescent emissions and the thermal stability of the framework. Multifunctional carboxylate building blocks[9] with special configurations, such as 1,4-benzenedicarboxylic acid (H_2bdc) with a 180° angle, are able to establish bridges between several metal centers through various coordination modes. A large number of metal−organic polymers with the H_2bdc ligand as an organic linker have been reported, and many of them show excellent physical properties. By taking into account such factors, we wondered if the linear bdc ligand would be incorporated into the lanthanide camphorate frameworks to mediate the skeleton. On the other hand, the H_2bdc ligand with its phenyl group endowed with a high-structuring effect and possessing electron-conjugate systems, may be a benign chromophore for the efficient luminescent sensitization of lanthanide ions. As a result, this substitution would lead to an increase of the total spin in the ground state.

On the basis of the above consideration, a synthetic strategy to fabricate new homochiral lanthanide camphorates with mixed achiral bdc ligands was carried out under solvothermal conditions. Successfully, seven multifunctional homochiral lanthanide camphorates $\{Ln_2(cam)_2(bdc)(H_2O)_2\}\cdot$ DMF (Ln = Sm, Eu, Gd, Tb, Dy, Ho, Er) were obtained and structurally characterized. Furthermore, luminescent and magnetic properties, thermogravimetric analyses (TGA), variable-temperature IR spectroscopy, and powder X-ray diffraction (PXRD) of some of these complexes were also studied.

Experimental Section

Materials and Instrumentation. All reagents were purchased commercially and used without further purification. All syntheses were carried out in 23 mL poly(tetrafluoroethylene)-lined stainless steel containers under autogenous pressure. Elemental analyses were performed on an EA1110 CHNS-0 CE elemental analyzer. Fourier transform infrared (FT-IR) spectra were measured as KBr pellets on a Nicolet Magna 750 FT-IR spectrometer in the range of 400−4000 cm^{-1}. All PXRD analyses were recorded on a Rigaku Dmax2500 diffractometer with Cu Kα radiation (λ = 1.540 56 Å) with a step size of 0.05°. The fluorescence spectra were measured on polycrystalline or powder samples at room temperature using an Edinburgh FLS920 TCSPC fluorescence spectrophotometer. The temperature dependencies of magnetic susceptibilities were performed on a Quantum Design PPMS model 600 magnetometer in the temperature range 2−300 K with an applied field of 1 kOe. Thermal stability studies were carried out on a NETSCHZ STA-449C thermoanalyzer with a heating rate of 10 °C/min under an air atmosphere.

Preparation of 1−7. A mixture of Ln_2O_3 (0.1 mmol, except 0.05 mmol of Tb_4O_7), D-H_2cam (0.3 mmol, 0.06 g), H_2bdc (0.2 mmol, 0.033 g), H_2O/DMF (10/2 mL), and HNO_3 (0.2 mmol) was sealed in a 25 mL Teflon-lined bomb, heated at 150 °C for 4 days under autogenous pressure, and then slowly cooled to room temperature. Prismatic air-stable crystals of **1**−**7** suitable for X-ray analyses were obtained. Crystals **2′** suitable for X-ray analyses were obtained by heating sample **2** at 200 °C for 30 min. These compounds were insoluble in common solvents, such as chloroform, acetonitrile, DMF, methanol, and ethanol. Their purities were also confirmed by experimental PXRD at room temperature (Figure S3 in the Supporting Information). Yield: ca. 42% (based on Sm) for **1**; 65% (based on Eu) for **2**; 60% (based on Gd) for **3**; 40% (based on Tb) for **4**; 62% (based on Dy) for **5**; 37% (based on Ho) for **6**; 30% (based on Er) for **7**. The general chemical formula sum is $C_{31}H_{43}Ln_2NO_{15}$. Anal. Calcd for **1**: C, 38.37; H, 4.47; N, 1.44. Found: C, 38.11; H, 4.82; N, 1.65. Eu. Anal. Calcd for **2**: C, 38.24; H, 4.45; N, 1.44. Found: C, 38.06; H, 4.93; N, 1.70. Anal. Calcd for **3**: C, 37.83; H, 4.40; N, 1.42. Found: C, 38.12; H, 4.63; N, 1.21. Anal. Calcd for **4**: C, 37.70; H, 4.39; N, 1.42. Found: C, 38.08; H, 4.55; N, 1.19. Anal. Calcd for **5**: C, 37.43; H, 4.36; N, 1.41. Found: C, 37.14; H, 4.52; N, 1.79. Anal. Calcd for **6**: C, 37.25; H, 4.34; N, 1.40. Found: C, 37.46; H, 4.61; N, 1.24. Anal. Calcd for **7**: C, 37.08; H, 4.32; N, 1.40. Found: C, 37.31; H, 4.15; N, 1.60. IR (KBr, cm^{-1}) for **1**: 3624.17 (s), 3347.94 (br), 2964.12 (s), 1669.18 (s), 1548.75 (vs), 1511.81 (s), 1463.92 (s), 1408.51 (s), 1390.47 (vs), 1315.99 (s), 1292.03 (s), 1171.82 (m), 1099.47 (m), 1021.15 (m), 924.66 (m), 815.45 (w), 802.29 (w), 746.67 (vs), 666.57 (w), 593.22 (w), 505.69 (m), 468.75 (w). IR (KBr, cm^{-1}) for **2**: 3622.56 (s), 3343.89 (br), 2964.41 (s), 1670.05 (s), 1552.63 (vs), 1511.37 (s), 1463.86 (s), 1411.22 (s), 1390.78 (vs), 1316.84 (s), 1292.85 (s), 1171.43 (m), 1099.65 (m), 1021.92 (m), 926.11 (m), 816.40 (w), 801.66 (w), 746.32 (vs), 665.44 (w), 593.29 (w), 505.53 (m),

(5) (a) Choppin, G. R.; Peterman, D. R. *Coord. Chem. Rev.* **1998**, *174*, 283. (b) Bunzli, J. C. G.; Piguet, C. *Chem. Soc. Rev.* **2005**, *34*, 1048. (c) Kido, J.; Okamoto, Y. *Chem. Rev.* **2002**, *102*, 2357. (d) Ma, L.; Evans, O. R.; Fowman, B. M.; Lin, W. B. *Inorg. Chem.* **1999**, *38*, 5837. (e) Dong, Y. B.; Wang, P.; Ma, J. P.; Zhao, X. X.; Wang, H. Y.; Tang, B.; Huang, R. Q. *J. Am. Chem. Soc.* **2007**, *129*, 4872. (f) Regulacio, M. D.; Pablico, M. H.; Vasquez, J. A.; Myers, P. N.; Gentry, S.; Prushan, M.; Tam-Chang, S. W.; Stoll, S. L. *Inorg. Chem.* **2008**, *47*, 1512. (g) Wang, C. M.; Wu, Y. Y.; Chang, Y. W.; Lii, K. H. *Chem. Mater.* **2008**, *20*, 2857. (h) Dissanayake, P.; Allen, M. J. *J. Am. Chem. Soc.* **2009**, *131*, 6342.

(6) (a) Ma, B. Q.; Zhang, D. S.; Gao, S.; Jin, T. Z.; Yan, C. H.; Xu, G. X. *Angew. Chem., Int. Ed.* **2000**, *39*, 3644. (b) Przychodzen, P.; Pelka, R.; Lewinski, K.; Supel, J.; Rams, M.; Tomala, K.; Sieklucka, B. *Inorg. Chem.* **2007**, *46*, 8924. (c) Alley, K. G.; Mukherjee, A.; Clerac, R.; Boskovic, C. *Dalton Trans.* **2008**, 59. (d) Sessoli, R.; Powell, A. K. *Coord. Chem. Rev.* **2009**, *253*, 2328. (e) De Silva, C. R.; Smith, S.; Shim, I.; Pyun, J.; Gutu, T.; Jiao, J.; Zheng, Z. P. *J. Am. Chem. Soc.* **2009**, *131*, 6336.

(7) (a) Reineke, T. M.; Eddaoudi, M.; Fehr, M.; Kelley, D.; Yaghi, O. M. *J. Am. Chem. Soc.* **1999**, *121*, 1651. (b) Dong, D. W.; Jiang, S. C.; Men, Y. F.; Ji, X. L.; Jiang, B. Z. *Adv. Mater.* **2000**, *12*, 646. (c) Plecnik, C. E.; Liu, S. M.; Shore, S. G. *Acc. Chem. Res.* **2003**, *36*, 499. (d) Devic, T.; Serre, C.; Audebrand, N.; Marrot, J.; Ferey, G. *J. Am. Chem. Soc.* **2005**, *127*, 12788. (e) Chandler, B. D.; Yu, J. O.; Cramb, D. T.; Shimizu, G. K. H. *Chem. Mater.* **2007**, *19*, 4467. (f) Nishiyabu, R.; Hashimoto, N.; Cho, T.; Watanabe, K.; Yasunaga, T.; Endo, A.; Kaneko, K.; Niidome, T.; Murata, M.; Adachi, C.; Katayama, Y.; Hashizume, M.; Kimizuka, N. *J. Am. Chem. Soc.* **2009**, *131*, 2151. (g) Mohapatra, S.; Hembram, K.; Waghmare, U.; Maji, T. K. *Chem. Mater.* **2009**, *21*, 5406.

(8) (a) Aspinall, H. C. *Chem. Rev.* **2002**, *102*, 1807. (b) Ngo, H. L.; Lin, W. B. *J. Am. Chem. Soc.* **2002**, *124*, 14298. (c) Thushari, S.; Cha, J. A. K.; Sung, H. H. Y.; Chui, S. S. Y.; Leung, A. L. F.; Yen, Y. F.; Williams, I. D. *Chem. Commun.* **2005**, 5515. (d) Yue, Q.; Yang, J.; Li, G. H.; Li, G. D.; Chen, J. S. *Inorg. Chem.* **2006**, *45*, 4431. (e) Lama, M.; Mamula, O.; Kottas, G. S.; Rizzo, F.; De Cola, L.; Nakamura, A.; Kuroda, R.; Stoeckli-Evans, H. *Chem.—Eur. J.* **2007**, *13*, 7358. (f) Yuan, G.; Shao, K. Z.; Wang, X. L.; Lan, Y. Q.; Du, D. Y.; Su, Z. M. *CrystEngComm* **2010**, *12*, 1147.

(9) (a) Wang, Z. Q.; Cohen, S. M. *J. Am. Chem. Soc.* **2007**, *129*, 12368. (b) Rosi, N. L.; Kim, J.; Eddaoudi, M.; Chen, B. L.; O'Keeffe, M.; Yaghi, O. M. *J. Am. Chem. Soc.* **2005**, *127*, 1504. (c) Du, M.; Jiang, X. J.; Zhao, X. J. *Chem. Commun.* **2005**, 5521. (d) Yang, J.; Yuo, Q.; Li, G. D.; Cao, J. J.; Li, G. H.; Chen, J. S. *Inorg. Chem.* **2006**, *45*, 2857. (e) Rowsell, J. L. C.; Millward, A. R.; Park, K. S.; Yaghi, O. M. *J. Am. Chem. Soc.* **2004**, *126*, 5666. (f) Loiseau, T.; Serre, C.; Huguenard, C.; Fink, G.; Taulelle, F.; Henry, M.; Bataille, T.; Ferey, G. *Chem.—Eur. J.* **2004**, *10*, 1373.

Table 1. Summary of Crystal Data and Structure Refinements for **1**−**7** and Eu-2′

	Sm-1	**Eu-2**	**Gd-3**	**Tb-4**
formula	$C_{31}H_{43}Sm_2NO_{15}$	$C_{31}H_{43}Eu_2NO_{15}$	$C_{31}H_{43}Gd_2NO_{15}$	$C_{31}H_{43}Tb_2NO_{15}$
fw	970.38	973.58	984.16	987.50
cryst syst	orthorhombic	orthorhombic	orthorhombic	orthorhombic
space group	$P2_12_12_1$	$P2_12_12_1$	$P2_12_12_1$	$P2_12_12_1$
a (Å)	12.9454(7)	12.957(4)	12.927(5)	12.932(8)
b (Å)	14.2341(8)	14.192(4)	14.084(6)	14.067(8)
c (Å)	19.0465(10)	19.006(5)	18.882(8)	18.928(12)
α (deg)	90	90	90	90
β (deg)	90	90	90	90
γ (deg)	90	90	90	90
V (Å^3)	3509.6(3)	3495.1(17)	3438(2)	3443(4)
Z	4	4	4	4
D_{calc} (mg/m^3)	1.836	1.850	1.902	1.905
μ (mm^{-1})	3.384	3.627	3.897	4.146
GOF on F^2	1.097	1.037	1.055	1.016
R1, wR2 [$I > 2\sigma(I)$]	0.0592, 0.1178	0.0354, 0.0665	0.0490, 0.0982	0.0720, 0.1918
R1, wR2 (all data)	0.0685, 0.1251	0.0384, 0.0680	0.0602, 0.1049	0.0809, 0.2009
Flack	−0.02(2)	0.000(13)	−0.056(19)	0.01(2)

	Dy-5	**Ho-6**	**Er-7**	**Eu-2′** (after heating **2** at 200 °C)
formula	$C_{31}H_{43}Dy_2NO_{15}$	$C_{31}H_{43}Ho_2NO_{15}$	$C_{31}H_{43}Er_2NO_{15}$	$C_{31}H_{43}Eu_2NO_{15}$
fw	994.66	999.52	1004.18	973.58
cryst syst	orthorhombic	orthorhombic	orthorhombic	orthorhombic
space group	$P2_12_12_1$	$P2_12_12_1$	$P2_12_12_1$	$P2_12_12_1$
a (Å)	12.939(3)	12.9406(6)	12.888(4)	12.967(5)
b (Å)	14.111(3)	14.1007(6)	14.048(4)	14.162(5)
c (Å)	18.910(4)	18.8914(8)	18.836(6)	18.984(6)
α (deg)	90	90	90	90
β (deg)	90	90	90	90
γ (deg)	90	90	90	90
V (Å^3)	3452.8(13)	3447.1(3)	3410.4(17)	3486(2)
Z	4	4	4	4
D_{calc} (mg/m^3)	1.913	1.926	1.956	1.855
μ (mm^{-1})	4.366	4.629	4.960	3.636
GOF on F^2	1.139	1.057	1.085	1.001
R1, wR2 [$I > 2\sigma(I)$][a]	0.0384, 0.0830	0.0514, 0.1247	0.0691, 0.1709	0.0389, 0.0692
R1, wR2 (all data)[a]	0.0416, 0.0853	0.0575, 0.1316	0.0763, 0.1777	0.0437, 0.0715
Flack	0.022(14)	0.037(18)	0.04(2)	0.016(15)

[a] $R1 = \sum||F_o| - |F_c||/\sum|F_o|$, $wR2 = \{\sum w(F_o^2 - F_c^2)2/\sum w(F_o^2)^2\}^{1/2}$; $w = 1/[\sigma^2(F_o^2) + (aP)^2 + bP]$, where $P = [\max(0,F_o^2) + 2F_c^2]/3$ for all data.

468.07 (w). IR (KBr, cm^{-1}) for **3**: 3622.83 (s), 3349.79 (br), 2964.93 (s), 1670.15 (s), 1555.62 (vs), 1512.13 (s), 1463.77 (s), 1411.45 (s), 1391.55 (vs), 1317.07 (s), 1293.03 (s), 1171.60 (m), 1099.83 (m), 1021.94 (m), 926.19 (m), 816.42 (w), 801.90 (w), 746.34 (vs), 671.85 (w), 594.42 (w), 505.56 (m), 468.56 (w). IR (KBr, cm^{-1}) for **4**: 3622.98 (s), 3371.54 (br), 2964.70 (s), 1670.22 (s), 1555.94 (vs), 1512.83 (s), 1463.77 (s), 1411.86 (s), 1388.09 (vs), 1317.06 (s), 1293.18 (s), 1171.67 (m), 1099.60 (m), 1022.35 (m), 926.73 (m), 817.19 (w), 802.18 (w), 746.39 (vs), 670.95 (w), 605.22 (w), 505.52 (m), 469.09 (w). IR (KBr, cm^{-1}) for **5**: 3620.73 (s), 3355.69 (br), 2965.09 (s), 1670.26 (s), 1557.66 (vs), 1514.65 (s), 1464.32 (s), 1413.13 (s), 1390.43 (vs), 1317.45 (s), 1293.65 (s), 1171.88 (m), 1099.74 (m), 1022.47 (m), 927.24 (m), 817.71 (w), 802.24 (w), 746.43 (vs), 667.95 (w), 597.30 (w), 505.61 (m), 468.02 (w). IR (KBr, cm^{-1}) for **6**: 3621.82 (s), 3323.73 (br), 2964.98 (s), 1670.22 (s), 1559.03 (vs), 1515.12 (s), 1464.40 (s), 1414.75 (s), 1391.65 (vs), 1317.76 (s), 1294.06 (s), 1172.03 (m), 1099.87 (m), 1022.99 (m), 927.85 (m), 817.52 (w), 802.67 (w), 746.54 (vs), 668.73 (w), 598.19 (w), 505.27 (m), 468.62 (w). IR (KBr, cm^{-1}) for **7**: 3620.66 (s), 3322.87 (br), 2963.99 (s), 1669.67 (s), 1553.68 (vs), 1512.27 (s), 1463.75 (s), 1411.14 (s), 1391.46 (vs), 1316.98 (s), 1292.99 (s), 1171.91 (m), 1099.80 (m), 1022.03 (m), 926.28 (m), 816.40 (w), 801.91 (w), 746.27 (vs), 668.38 (w), 595.33 (w), 505.91 (m), 468.45 (w).

Single-Crystal Structure Determination. Suitable single crystals of compounds **1**−**7** and **2**′ (heating **2** at 200 °C for 30 min) were carefully selected under an optical microscope and glued to thin glass fibers. Single-crystal X-ray diffraction intensities of complexes **2**, **2**′, **3**, and **6** were collected on a Rigaku SCXmini CCD diffractometer, those of **1** and **5** on a Rigaku Mercury CCD diffractometer; **4** and **7** were performed with a Saturn 70 CCD diffractometer at 293(2) K. All diffractometers were equipped with graphite-monochromated Mo Kα radiation (λ = 0.710 73 Å). The intensity data sets were collected with the ω-scan technique and reduced by *CrystalClear* software. The structure was solved by direct methods and expanded with Fourier techniques. Empirical absorption corrections were applied to the data using the *SADABS* program.[10] The structures were solved by direct methods and refined by full-matrix least squares on F^2 using the *SHELXTL-97* program.[11] All nonhydrogen atoms were refined anisotropically, the hydrogen atoms bound to carbon were located by geometrical calculations, and their positions and thermal parameters were fixed during structural refinement. However, the H_{2WB} atom bonding to the coordinated water molecule O_{2W} atom lacks the appropriate oxygen atom in the neighborhood to form a hydrogen bond. All calculations were performed with the *SHELXL-97* package. Pertinent crystallographic data and structural refinements for **1**−**7** and **2**′ are listed in Table 1. The selected bond distances of these isostructural lanthanide camphorates are listed in Table S1 in the Supporting Information.

(10) Sheldrick, G. M. *SADABS, Program for Area Detector Adsorption Correction*; Institute for Inorganic Chemistry, University of Göttingen: Göttingen, Germany, 1996.

(11) Sheldrick, G. M. *SHELXL-97, Program for Solution of Crystal Structures*; Institute for Inorganic Chemistry, University of Göttingen: Göttingen, Germany, 1997.

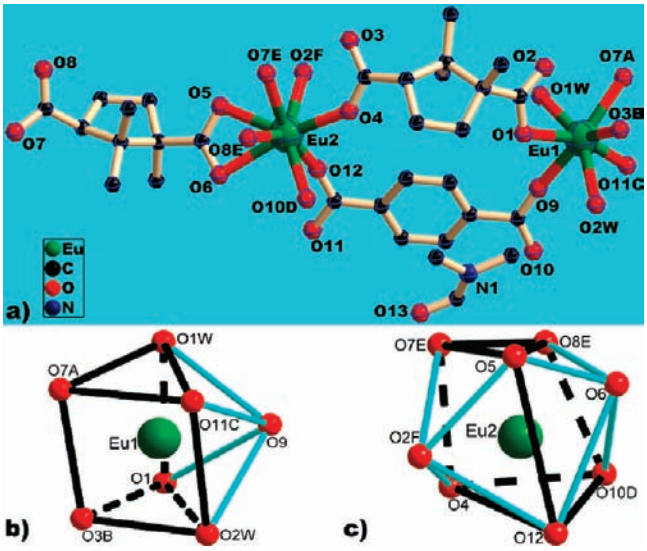

Figure 1. (a) Perspective view of the coordination environment of Eu^{III} centers of compound **2**. (b) Distorted monocapped trigonal-prismatic coordination polyhedron of the $Eu1^{III}$ ion. (c) Distorted dicapped trigonal-prismatic coordination polyhedron of the $Eu2^{III}$ ion. Symmetry codes: A, $1+x, -1+y, z$; B, $-1-x, -0.5+y, 0.5-z$; C, $0.5+x, 2.5-y, -z$; D, $-0.5+x, 2.5-y, -z$; E, $-2-x, -0.5+y, 0.5-z$; F, $-1-x, 0.5+y, 0.5-z$. All hydrogen atoms have been omitted for clarity.

Results and Discussion

Description of the Structures. Single-crystal X-ray structure analyses reveal that prism crystals **1**−**7** are isostructural. Attempts to synthesize more isomorphous complexes except **1**−**7** with other lanthanide ions were unsuccessful, which may be due to the effect of lanthanide contraction.[12] Here, only the structure of complex **2** as a representative is described in detail. As depicted in Figure 1, the asymmetric unit of **2** contains two crystallographically unique Eu^{III} ions, two cam groups, one bdc ligand, two coordinated water molecules, and one DMF molecule. The Eu1 site is seven-coordinated, with five oxygen atoms from three cam and two bdc molecules, and two-coordinated water molecules, to form distorted monocapped trigonal-prismatic coordination geometry. While the eight-coordinated Eu2 ion adopts a distorted bicapped triprismatic coordination mode, which bonds to six oxygen donors from four cam ligands, the two remnant sites are occupied by two symmetry-related bdc ligands. The Eu−O bond lengths vary from 2.319 to 2.638 Å, while the Eu−O_{H_2O} bonds are in the medial distances of 2.374 and 2.405 Å. All of the Ln−O distances are in the ranges compatible with the values of the previously published series of lanthanide complexes[13] with carboxylic acids as bridging ligands.

Scheme 1. Crystallographically Established Coordination Modes of the Organic Ligands (**I**, cam-1; **II**, cam-2; **III**, bdc) in Lanthanide Camphorates **1**−**7**

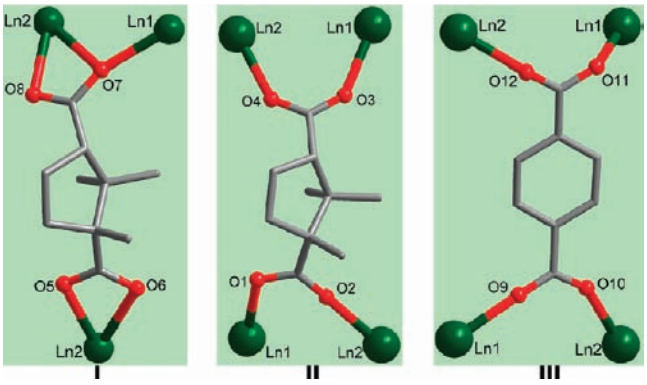

To understand the structure, it is preferable to differentiate the two crystallographically independent cam ligands as cam-1 and cam-2, respectively. Interestingly, the cam-1 and cam-2 ligands display μ_3-$\kappa^1,\kappa^1,\kappa^2,\kappa^1$ and μ_4-$\kappa^1,\kappa^1,\kappa^1,\kappa^1$ coordination modes, respectively, as shown in Scheme 1. The cross-linking of pseudo-paddle-wheel units by D-cam ligands results in the formation of a homochiral gridlike (4,4)-layered substructure perpendicular to the *c* axis (Figure S1 in the Supporting Information). However, the overall structure is comprised of Eu−O−C rods, which are rather more complex than some rods described by others previously. Six carboxylate groups join the alternating seven- and eight-coordinated dinuclear europium centers with Eu···Eu distances of 4.1232 and 5.4779 Å to form infinite $\{Eu_2(OCO)_6(H_2O)_2\}_n$ secondary building units (SBUs) running along the *c* axis (Figure 2). These rod-shaped SBUs are further extended into the final three-dimensional (3D) open framework, where each one-dimensional (1D) inorganic chain is connected to four neighboring parallel rods by cam linkers, with the auxiliary bdc ligands serving as pillars. This arrangement leaves an incommodious void because the methyl groups on the ring of the D-cam ligands protrude into the open space of the 3D framework $\{Ln_2(cam)_3(bdc)(H_2O)_2\}$. Calculations using the *PLATON* program[14] show that the total solvent-accessible volume is approximately 628.6 $Å^3$ per unit cell, comprising 17.9% of the unit cell volume. The free DMF molecules act as guests settled into the apertures of the framework. Apparently, intercalation of the DMF molecules plays a vital template role in the reinforcement of the 3D rare-earth open framework. More importantly, strong hydrogen-bonding interactions exist between the water and DMF molecules, giving rise to a reinforcement of the 3D framework arrangement. The detailed geometric parameters for the hydrogen bonds are listed in Table 2.

Luminescent Properties. The solid-state luminescent properties of the as-synthesized samples **1**, **2**, **4**, and **5**

(12) (a) Dimos, A.; Tsaousis, D.; Michaelides, A.; Skoulika, S.; Golhen, S.; Ouahab, L.; Didierjean, C.; Aubry, A. *Chem. Mater.* **2002**, *14*, 2616. (b) Hughes, I. D.; Dane, M.; Ernst, A.; Hergert, W.; Luders, M.; Poulter, J.; Staunton, J. B.; Svane, A.; Szotek, Z.; Temmerman, W. M. *Nature* **2007**, *446*, 650. (c) Taylor, K. N. R.; Darby, M. I. *Physics of Rare Earth Solids*; Chapman and Hall: London, 1972; p 60. (d) Seitz, M.; Oliver, A. G.; Raymond, K. N. *J. Am. Chem. Soc.* **2007**, *129*, 11153. (e) Liu, Q. Y.; Xu, L. *Eur. J. Inorg. Chem.* **2005**, 3458. (f) Liu, Q. D.; Gao, S.; Li, J. R.; Ma, B. Q.; Zhou, Q. Z.; Yu, K. B. *Polyhedron* **2002**, *21*, 1097. (g) Pan, L.; Huang, X. Y.; Li, J.; Wu, Y. G.; Zheng, N. W. *Angew. Chem., Int. Ed.* **2000**, *39*, 527.

(13) (a) Yin, P. X.; Li, Z. J.; Zhang, J.; Zhang, L.; Lin, Q. P.; Qin, Y. Y.; Yao, Y. G. *CrystEngComm* **2009**, *11*, 2734. (b) Wang, J. G.; Huang, C. C.; Huang, X. H.; Liu, D. S. *Cryst. Growth Des.* **2008**, *8*, 795. (c) Sun, Y. Q.; Zhang, J.; Yang, G. Y. *Chem. Commun.* **2006**, 1947. (d) Cheng, J. W.; Zhang, J.; Zheng, S. T.; Yang, G. Y. *Chem.—Eur. J.* **2008**, *14*, 88. (e) Huang, Y. G.; Jiang, F. L.; Yuan, D. Q.; Wu, M. Y.; Gao, Q.; Wei, W.; Hong, M. C. *J. Solid State Chem.* **2009**, *182*, 215. (f) Li, Y.; Xu, G.; Zou, W. O.; Wang, N. S.; Zheng, F. K.; Wu, M. F.; Zeng, H. Y.; Guo, G. C.; Huang, J. S. *Inorg. Chem.* **2008**, *47*, 7945. (g) Kiritsis, V.; Michaelides, A.; Skoulika, S.; Golhen, S.; Ouahab, L. *Inorg. Chem.* **1998**, *37*, 3407.

(14) Spek, A. L. *Acta Crystallogr., Sect. A* **1990**, *46*, C34.

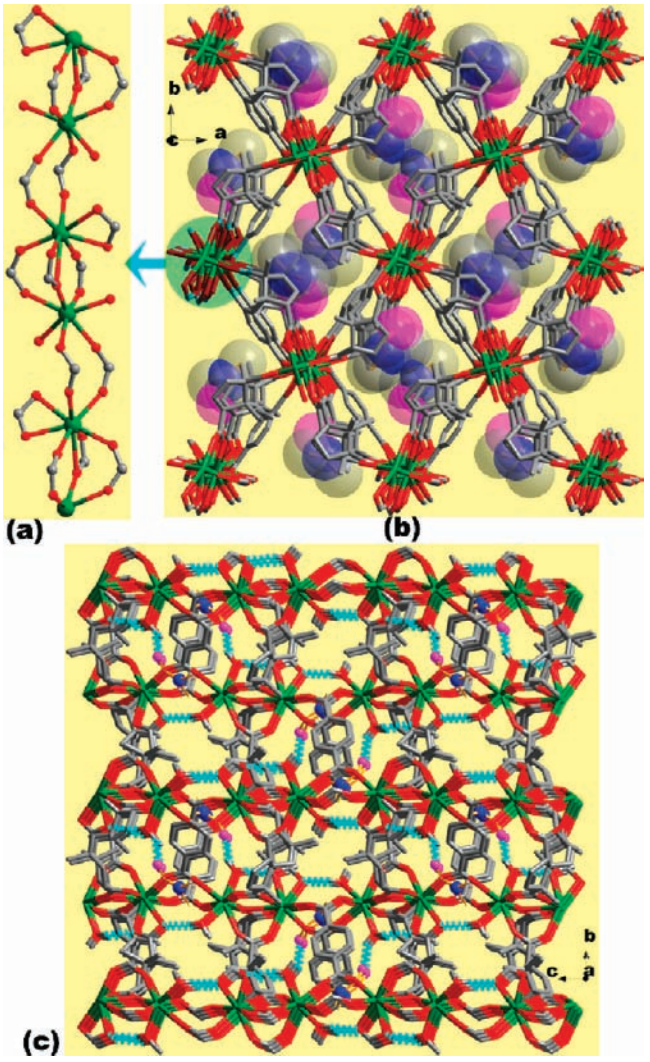

Figure 2. (a) Ball-and-stick representation of a 1D inorganic rod-shaped chain of $\{Eu_2(OCO)_6(H_2O)_2\}_n$ (all of the hydrogen atoms were omitted). (b) Schematic view of the 3D open framework of **2** along the *c* axis. The space-filling models represent DMF host molecules trapped in the apertures. (c) 3D framework of **2** viewed along the *bc* plane. All of the hydrogen bonds between O−H···O atoms are denoted with dashed cyan lines.

Table 2. Hydrogen-Bonding-Parameter Donor/Acceptor Scheme (Å and deg) for **2**[a]

D−H···A	H···A	D···A	∠DHA
O1W−H1WA···O13#1	1.84	2.604(6)	149.2
O1W−H1WB···O4#1	2.04	2.698(6)	134.1
O2W−H2WA···O3#2	1.86	2.671(6)	158(8)

[a] Symmetry transformations used to generate equivalent atoms for **2**: #1, $x+2$, $y-{}^1/_2$, $-z+{}^3/_2$; #2, $x-{}^1/_2$, $-y+{}^1/_2$, $-z+2$.

and the free H_2bdc ligand were investigated at room temperature. The emission spectra of the four complexes (Figure 3) exhibit the characteristic emission of Sm^{3+}, Eu^{3+}, Tb^{3+}, and Dy^{3+}, respectively. For compound **1**, the emission peaks at 562, 598, 652, and 708 nm are attributed to the emissions of $4G_{5/2} \rightarrow 6H_J$ ($J = {}^5/_2, {}^7/_2, {}^9/_2$, and ${}^{11}/_2$) transitions for the Sm^{III} ions. The emission peaks of compound **2** occurred at 592, 616, 650, and 700 nm, which can be assigned to $5D_0 \rightarrow 7F_J$ ($J = 1-4$) transitions, respectively. The symmetric forbidden emission $5D_0 \rightarrow 7F_0$ at 580 nm is invisible in **2**. The most intense emission at 616 nm is attributed to the electric-dipole-induced $5D_0 \rightarrow 7F_2$ transition, which is hypersensitive to the coordination environment of the Eu^{III} ions and implies a red emission light of **2**. The medium-strong emission at 592 nm corresponds to the magnetic-dipole-induced $5D_0 \rightarrow 7F_1$ transition, which is fairly insensitive to the environment of the Eu^{III} ions. The intensity ratio of 3.63 for $I(5D_0 \rightarrow 7F_2):I(5D_0 \rightarrow 7F_1)$ indicates that the symmetry of the Eu^{III} ion site is low and Eu^{3+} ions in **2** are not all located at the inversion center,[15,16] which is in good agreement with the result of single-crystal X-ray analysis. Compound **4** emits green light and displays a characteristic emission transition of $5D_4 \rightarrow 7F_J$ ($J = 3-6$) of the Tb^{3+} ion. Two intense emission bands at 490 and 544 nm correspond to electronic transitions from the excited state $^5D_4$ to the multiplets $^7F_6$ and $^7F_5$, while the weaker emission bands at 586 and 621 nm originate from $5D_4 \rightarrow 7F_4$ and $5D_4 \rightarrow 7F_3$. For compound **5**, the peaks at 481 and 574 nm can be assigned to $^4F_{9/2} \rightarrow {}^6H_{15/2}$ (~470 nm) and $^4F_{9/2} \rightarrow {}^6H_{13/2}$ (~570 nm) transitions. The $^4F_{9/2} \rightarrow {}^6H_{13/2}$ transition is clearly stronger than the $^4F_{9/2} \rightarrow {}^6H_{15/2}$ transition. The corresponding decay lifetimes are 1212.4, 496.2, 3.82, and 0.859 μs, and the photoluminescence efficiencies are 63.68%, 23.59%, 5.19%, and 3.04% for complexes **4**, **2**, **1**, and **5**, respectively, which are comparable to other corresponding Ln^{III} complexes.[16,17]

For the H_2bdc ligand, the emission peak at 383 nm among the emission bands in the region 350−450 nm can be assigned to the intraligand $\pi^* \rightarrow \pi$ or $\pi^* \rightarrow$ n transition. However, upon complexation with Ln^{III} ions, only characteristic emission spectra associated with the corresponding Ln^{III} ions were observed. The absence of the ligand-based emission in the fluorescence bands of the four compounds indicates that energy transfer from the ligand to the Ln^{III} center is effective during photoluminescence.

Magnetic Properties. Temperature-dependent magnetic susceptibilities of **2**, **3**, and **5** were measured in the temperature range 2−300 K. As shown in Figure 4, they display different magnetic behaviors, owing to the unique magnetic nature of respective rare-earth species. Theoretically, compared with **3**, it is more difficult to analyze the magnetic properties of **2** and **5** because of two effects, namely, (i) the spin−orbit coupling, which partially removes the $2J + 1$ degeneracy of the ground state in zero field, further splitting into Stark levels by the crystal-field perturbation, and (ii) the thermal population of free-ion excited states, which happens with Eu^{3+} and Sm^{3+}.[18,19]

(15) (a) Bunzli, J.-C. G.; Choppin, G. R. *Lanthanide Probes in Life, Chemical and Earth Sciences: Theory and Practice*; Elsevier Scientific Publishers: Amsterdam, The Netherlands, 1989. (b) Guo, X. F.; Feng, M. L.; Xie, Z. L.; Li, J. R.; Huang, X. Y. *Dalton Trans.* **2008**, 3101.
(16) Cheng, J. W.; Zheng, S. T.; Ma, E.; Yang, G. Y. *Inorg. Chem.* **2007**, *46*, 10534.
(17) (a) Quici, S.; Cavazzini, M.; Marzanni, G.; Accorsi, G.; Armaroli, N.; Ventura, B.; Barigelletti, F. *Inorg. Chem.* **2005**, *44*, 529. (b) Huang, Y. G.; Wu, B. L.; Yuan, D. Q.; Xu, Y. Q.; Jiang, F. L.; Hong, M. C. *Inorg. Chem.* **2007**, *46*, 1171.
(18) Andruh, M.; Bakalbassis, E.; Kahn, O.; Trombe, J. C.; Porcher, P. *Inorg. Chem.* **1993**, *32*, 1616.
(19) (a) Li, Y.; Zheng, F. K.; Liu, X.; Zou, W. Q.; Guo, G. C.; Lu, C. Z.; Huang, J. S. *Inorg. Chem.* **2006**, *45*, 6308. (b) Gurek, A. G.; Basova, T.; Luneau, D.; Lebrun, C.; Kol'tsov, E.; Hassan, A. K.; Ahsen, V. *Inorg. Chem.* **2006**, *45*, 1667.

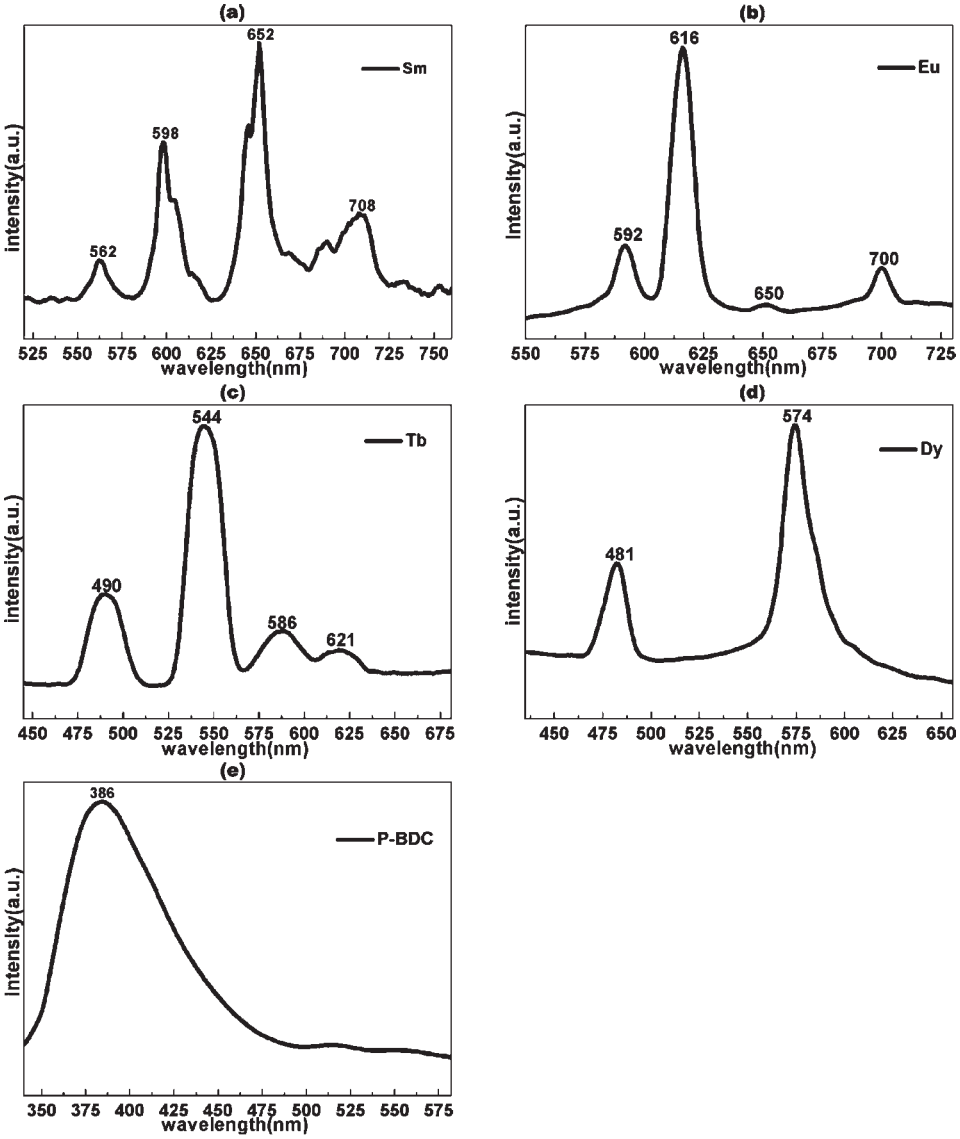

Figure 3. Emission spectra of compounds **1** (excited at 280 nm) (a), **2** (excited at 255 nm) (b), **4** (excited at 255 nm) (c), and **5** (excited at 315 nm) (d) and the free H_2bdc ligand (excited at 335 nm) (e) in the solid state at room temperature.

At 300 K, the observed $\chi_m T$ value of compound **2** is 2.84 $cm^3 \cdot K/mol$, slightly lower than the theoretical value (3.06 $cm^3 \cdot K/mol$) of two isolated Eu^{3+} ions calculated by Van Vleck allowing for population of the first three low-lying states with the energies 0, λ, and 3λ.[20] The $\chi_m T$ value decreases steeply and is close to zero at 2 K, which should be mainly ascribed to the depopulation of the levels with nonzero J values and a $J = 0$ ground state of the Eu^{3+} ion ($^7F_0$), also reflected in the small value of the Weiss-like constant θ (−0.14 K) on the basis of the equations deduced from the Eu^{3+} ion in the monomeric system with the free-ion approximation.[18]

For compound **3**, the situation is much simpler, in which none of the crystal-field effect, the spin−orbit coupling, and the thermally populated excited states need to be considered. The plot of χ_m^{-1} vs T over the whole temperature range obeys the Curie−Weiss law with $\theta = -0.140$ K and $C = 15.85$ $cm^3 \cdot K/mol$, which is consistent with the expected value for a binuclear compound of gadolineum (15.85 $cm^3 \cdot K/mol$). The $\chi_m T$ value at room temperature is equal to 15.87 $cm^3 \cdot K/mol$; upon lowering of the temperature, $\chi_m T$ remains almost constant until 15 K and then falls rapidly. Fitting the experimental data to eq 1 derived by Fisher[21] for an $S = {}^7/_2$ alternating Heisenberg chain, $\{u_i = \coth[J_i S(S+1)/k_B T] - [k_B T/J_i S(S+1)]$ $(i = 1$ and 2 and $S = {}^7/_2)\}$

$$\chi_{chain} = \frac{Ng^2\mu_B{}^2 S(S+1)}{3k_B T}\left(\frac{1+u_1+u_2+u_1u_2}{1-u_1u_2}\right) \quad (1)$$

$$\chi_m = \frac{\chi_{chain}}{1 - 2zJ\chi_{chain}/Ng^2\mu_B{}^2} \quad (2)$$

where N, g, μ_B, and k_B have their usual meanings, J_1 and J_2 account for the intrachain alternating coupling

(20) (a) Wan, Y. G.; Zhang, L. P.; Jin, L. P.; Gao, S.; Lu, S. Z. *Inorg. Chem.* **2003**, *42*, 4985. (b) Sun, Y. Q.; Zhang, J.; Chen, Y. M.; Yang, G. Y. *Angew. Chem., Int. Ed.* **2005**, *44*, 5814.

(21) Fisher, M. E. *Am. J. Phys.* **1964**, *32*, 343.

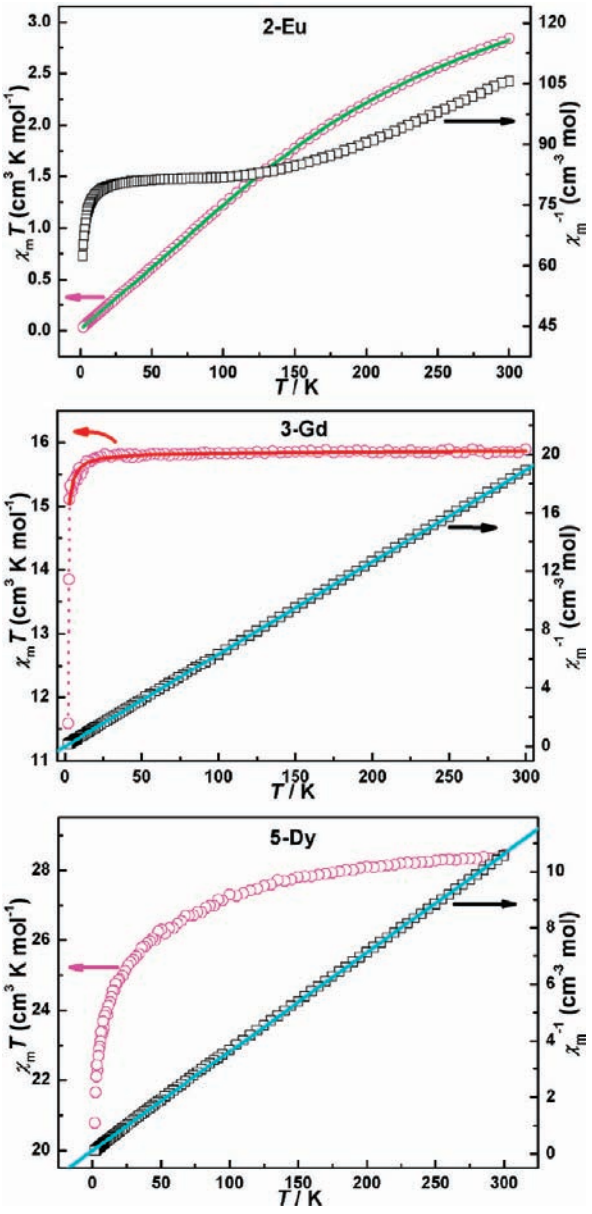

Figure 4. Temperature dependence of $\chi_m T$ and χ_m^{-1} vs T for **2**, **3**, and **5**. The solid green line in **2** denotes the fitting of $\chi_m T$ vs T (λ = 537.7 cm^{-1} and θ = −0.14 K) on the basis of the equations deduced from the Eu^{3+} ion in the monomeric system with the free-ion approximation. The solid red line in **3** shows the best fit obtained by using a 1D alternating Fisher model. The solid cyan lines in **3** and **5** represent the best fittings of the experimental data based on the theoretical model described by the Curie−Weiss law (for χ_m^{-1}).

constants, and the interchain interaction (zJ) was also considered, leading to $J_1 = J_2 = -0.000\,03$ cm^{-1}, $zJ = -0.015$ cm^{-1}, and $g = 2.00$ with an agreement factor R ($R = \sum[(\chi_m T)_{obs} - (\chi_m T)_{calc}]^2/\sum[(\chi_m T)_{obs}]^2$) of 1.2×10^{-3}. Such behavior can be attributed to a lack of obvious interactions between metallic centers, which is typical of paramagnetic behavior.

The corrected $\chi_m T$ value of compound **5** per formula unit is 28.44 cm^3·K/mol at 300 K, corresponding well to the expected value 28.54 cm^3·K/mol, which is calculated by the formula $\chi_m T = N\beta^2 g_{Ln}{}^2 J_{Ln}(J_{Ln} + 1)/3k$ for two magnetically insulated Dy^{3+} ions with a $^6H_{15/2}$ ground state. Upon cooling, the $\chi_m T$ product decreases monotonically

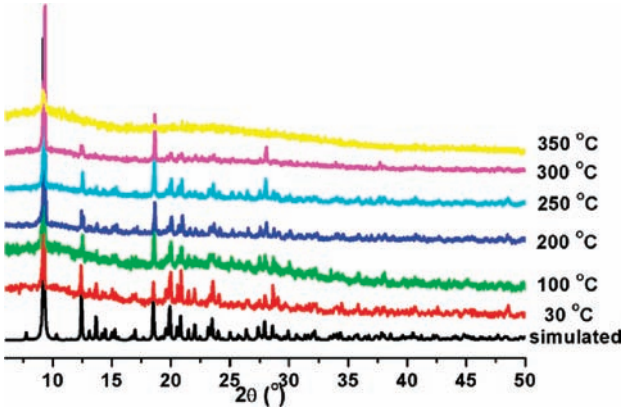

Figure 5. Variable-temperature PXRD patterns for compound **Eu-2**.

and finally drops to a value of 11.59 cm^3·K/mol at 2 K. Fitting of the data (χ_m^{-1} vs T) according to the Curie−Weiss law gives Weiss constants (θ) of −3.19 K in the whole temperature range. Such magnetic behaviors of a decrease of $\chi_m T$ and a negative value of θ, typical for Ln^{3+} complexes, are primarily due to splitting of the ligand field of the Ln^{3+} ions as a result of strong spin−orbit coupling and are partly attributed to possible antiferromagnetic intradimer coupling.

PXRD Patterns and Thermal Stability Analyses. The simulated and experimental PXRD patterns of compounds **1**−**7** obtained at room temperature are shown in Figure S3 in the Supporting Information. Their peak positions correspond well with each other, indicating the phase purity of the solids. The difference in reflection intensities between the simulated and experimental patterns may be due to variation in the preferred orientation of the powder samples during collection of the experimental PXRD data.

Basically, analogous structure types exhibit similar thermal behavior.[22] The thermal behavior of complex **2** was studied in a dynamic air atmosphere for single-phase polycrystalline samples from 30 to 1200 °C at a heating rate of 10 °C/min (Figure S4 in the Supporting Information). It shows simple thermal behavior and merely undergoes one step of weight loss. As shown in Figure 5, the experimental variable-temperature PXRD of **2** after calcination at elevated temperature in the range of 35−300 °C is still in good agreement with the calculated one of **2**, indicating that the crystal lattice of **2** still remains intact at 300 °C. In other words, the departure of the guest DMF molecules and coordinated water molecule does not lead to an obvious phase transformation. It is worth noting that **2′** still remains in a single-crystal state after heating of **2** at 200 °C. When the sample is heated at 350 °C, the long-range order of the structure is lost and forms an amorphous phase. The guest DMF molecules and two coordinated water molecules were completely lost for **2** from stoichiometry calculations (calcd/found: 11.09/11.27%) at 480 °C. After that, the sharp weight loss above 480 °C corresponds to decomposition of the organic cam

(22) (a) Chen, L. F.; Zhang, J.; Ren, G. Q.; Li, Z. J.; Qin, Y. Y.; Yin, P. X.; Cheng, J. K.; Yao, Y. G. *CrystEngComm* **2008**, *10*, 1088. (b) Liu, L.; Sun, Z. G.; Zhang, N.; Zhu, Y. Y.; Zhao, Y.; Lu, X.; Tong, F.; Wang, W. N.; Huang, C. Y. *Cryst. Growth Des.* **2010**, *10*, 406. (c) Cheng, J. W.; Zheng, S. T.; Liu, W.; Yang, G. Y. *CrystEngComm* **2008**, *10*, 1047.

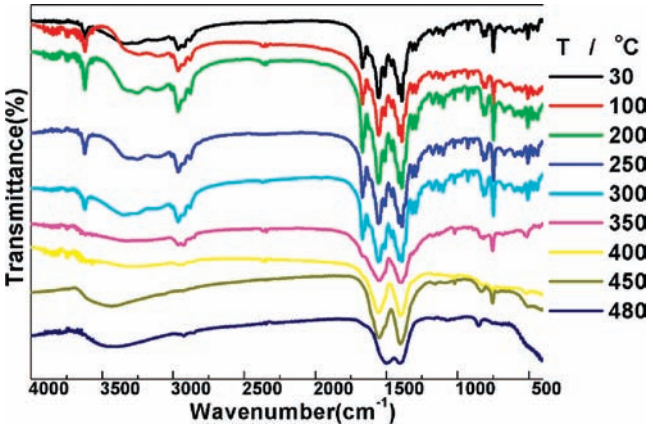

Figure 6. Variable-temperature IR spectra for compound **Eu-2**.

and bdc ligands. Until 1200 °C, the remaining weight of 34.66% corresponds to the percentage of Eu and O components, Eu_2O_3 (calcd: 36.15%).

These relative conclusions were corroborated by variable-temperature IR spectroscopy for the as-synthesized sample **2** and the thermal decomposition residue at each stage of 100−480 °C (Figure 6). The IR spectra of these samples heated from room temperature to 300 °C were found to be broadly similar to that observed for the original product. However, upon prolonged heating of compound **2** at 350 °C, a distinct change of the IR spectra occurred. On the one hand, IR spectra confirm the removal of the water molecule coordinated to the metal, from a loss of the sharp picks around 3622, 3343, and 2964 cm^{-1}.[23] On the other hand, we find nearly a total disappearance of the strong band centered at 1670 cm^{-1}, which is ascribed to the vibration peak of C=O in free DMF molecules.[24] In addition, these compounds show identical IR spectra, with the absorption bands of the asymmetric and symmetric stretching modes of the carboxylate frequency appearing around 1552 and 1390 cm^{-1}, respectively. After 480 °C, all of the peaks disappeared, accompanying the removal of those coordinated organic species, and the whole framework completely collapsed.

(23) (a) Hix, G. B.; Harris, K. D. M. *J. Mater. Chem.* **1998**, *8*, 579. (b) Yaghi, O. M.; Li, H. L.; Groy, T. L. *J. Am. Chem. Soc.* **1996**, *118*, 9096. (c) Nag, A.; Lotsch, B. V.; der Gunne, J. S. A.; Oeckler, O.; Schmidt, P. J.; Schnick, W. *Chem.—Eur. J.* **2007**, *13*, 3512.

(24) (a) Niu, J. Y.; Guo, D. J.; Wang, J. P.; Zhao, J. W. *Cryst. Growth Des.* **2004**, *4*, 241. (b) Wang, J. P.; Zhao, J. W.; Duan, X. Y.; Niu, J. Y. *Cryst. Growth Des.* **2006**, *6*, 507.

Conclusion

In summary, a series of multifunctional homochiral lanthanide camphorates with mixed achiral bdc ligands have been successfully obtained from solvothermal synthesis. The results present the first example of homochiral lanthanide camphorates adopting 3D open frameworks constructed from rod-shaped $[Ln_2(OCO)_6(H_2O)_2]_n$ SBUs. It is of interest that two combination strategies are successfully applied here. One is the combination of an enantiopure D-cam ligand with an achiral bdc ligand, which brings both homochirality and rigidity into the lanthanide materials. Another is the combination of homochirality and magnetism or luminescence for the lanthanide materials; the interesting luminescent and magnetic properties presented by the reported compounds reveal that they are potential multifunctional materials with special chiral photoactive or magnetic applications.

Acknowledgment. This work was supported by the 973 Program of China (Grants 2007CB815302 and 2009CB939803), the Chinese Academy of Sciences (Grants KJCX2.YW.319, KJCX2.YW.M10, and KJCX2-YW-M05), the Knowledge Innovation Program of the Chinese Academy of Sciences, and the Fund of Fujian Key Laboratory of Nanomaterials (Grant 2006L2005).

Supporting Information Available: Crystallographic data in CIF format, table of selected bond lengths, a TGA curve, simulated and experimental PXRD patterns, and additional structural plots. This material is available free of charge via the Internet at http://pubs.acs.org. The atomic coordinates for this structure have also been deposited with the Cambridge Crystallographic Data Centre as CCDC reference numbers 759346−759352. The coordinates can be obtained, upon request, from the Director, Cambridge Crystallographic Data Centre, 12 Union Road, Cambridge CB2 1EZ, U.K.